Valence Distributions of Iron and Manganese in Pure, Manganese-doped and Calcium-doped Yttrium Orthoferrite

CAO, Xue-Qiang(曹学强) ZENG, Yue*(曾跃)
College of Chemistry and Chemical Engineering, Hunan Normal University, Changsha, Hunan 410081, China

The valence distributions of Fe and Mn in yttrium orthoferrite ($YFeO_3$), $YFe_{0.6}Mn_{0.4}O_3$ and $Y_{0.9}Ca_{0.1}Fe_{0.6}Mn_{0.4}O_{3-\delta}$ were studied by the measurement of thermal power. Pure $YFeO_3$ shows the n-type electrical conductivity associated with small polaron hopping between Fe^{2+} and Fe^{3+}. Both $YFe_{0.6}Mn_{0.4}O_3$ and $Y_{0.9}Ca_{0.1}Fe_{0.6}Mn_{0.4}O_{3-\delta}$ show n-type and p-type conductivities at high and low temperatures respectively associated with small polaron hopping between Mn^{3+} and Mn^{4+}, iron has only oxidation state of Fe^{3+} and does not have contribution to the electrical conductivity.

Keywords Valence distribution, yttrium orthoferrite, doping, thermal power

Introduction

The perovskite-structured lanthanum-transition metal oxides doped with alkaline earth metals, *i.e.* $La_{1-x}A_xMO_{3-\delta}$ (A = Ca, Sr; M = Mn, Fe, Cr, Co) are of technological importance for the application in Solid Oxide Fuel Cells (SOFCs), chemical sensors and catalysts.[1,2] One of themost promising cathode materials for SOFC is $La_{1-x}Sr_xMnO_{3-\delta}$, even though it has some disadvantages such as formation of high-resistance $La_2Zr_2O_7$ and $SrZrO_3$ with yttrium stabilized zirconia (YSZ), chemical instability at high temperature and under low oxygen pressure, and diffusion of Mn into YSZ.[3] $Y_{1-x}Ca_xFeO_{3-\delta}$ is a newly proposed and promising cathode material for SOFC.[1,4] This material has high phase stability and comparable thermal expansion coefficient with YSZ, but its electrical conductivity is still not high enough for practical application. $Y_{1-x}Ca_xMnO_{3-\delta}$ has very high electrical conductivity, however, its microcracking problem and instability under low oxygen pressure make it useless in SOFC.[3,5] The search for materials possessing the structural stability and electrical conductivity required in the fuel-cell environment has led to the investigation of mixed systems. Recently studied examples are $Y(Cr,Mn)O_3$,[6] $La(Cr,Mn)O_3$,[6,7] $(La,Sr)(Cr,Mn)O_3$,[8] $(La,Sr)(Co,Fe)O_3$[9] and $(La,Sr/Ca,Ba)(Co,Fe)O_3$.[10,11] In the previous work,[12] the electrical property of $Y_{1-x}Ca_xFe_{1-y}Mn_yO_{3-\delta}$ ($x \leq 0.1$, $y \leq 0.4$) was studied. The substitutions of Mn for Fe and Ca for Y lead to a great increase of conductivity, but the valence distributions of Fe and Mn were not confirmed. The thermal power, namely, Seebeck-coefficient measurement has been successfully applied to study the conductivity mechanism and to distinguish oxidation states of Mn in Mn_3O_4,[13] Fe in Fe_3O_4-$FeAl_2O_3$/Fe_2TiO_4/$CoFe_2O_4$[14-16] and $(Mn_yCo_{1-y})_{0.4}Fe_{2.6}O_4$,[17] and valence distributions in spinels.[18] In this work, we study the valence distribution with the help of thermal power measurement, and it is believed that this method is helpful for the further understanding of conductivity mechanism in the doped materials.

Experimental

Most of chemicals used in this work were of A.R. grade (>99.9%). All samples were prepared by solid state reaction method. Stoichiometric mixtures of corresponding metal oxides or carbonates were calcinated at 900℃ for 10 h. The product was milled with zirconia ball for 24 h and followed by cold-isostatically pressing and sintering at 1350℃ for 15 h. Phase purity and crys-

* E-mail: zengyue@public.cs.hn.cn
Received April 28, 2000; accepted November 15, 2000.

tal structure of each composition were examined by XRD (X-ray powder diffraction, XRD-2000, Scintag Inc.) using Cu $K\alpha_1$ radiation. DC-electrical conductivity measurement was carried out by means of four-probe technique (Keithley 220 programmable current source and 2000 multimeter). The Seebeck-coefficient was determined by applying a temperature gradient of maximum 10 K along the length of the specimen and repeating the measurement of the temperature difference and the corresponding Seebeck voltage. At least 20 experimental points were taken, andthe slope of the resulting line gave the Seebeck-coefficient. The oxygen partial pressure was controlled by a gas mixture of N_2/O_2 or CO_2/CO and monitored with a YSZ oxygen sensor. The specimen size was about 1.8 mm × 1.8 mm × 20 mm.

Results and discussion

Synthesis of $YFeO_3$ *and* $Y_{1-x}Ca_xFe_{1-y}Mn_yO_{3-\delta}$

$Y_3Fe_5O_{12}$ (garnet) is often found to co-existing with $YFeO_3$. In order to synthesize $YFeO_3$ in which the $Y_3Fe_5O_{12}$ content is as low as possible, it is necessary to investigate the formation mechanism of $YFeO_3$. Two mechanisms for its formation with Y_2O_3 and Fe_2O_3 as starting materials are proposed. Some thermal chemical data related to the formations of $YFeO_3$ and $Y_3Fe_5O_{12}$ are listed in Table 1. The calculation of Gibbs-free energy changes of the following reactions was based on those data.

Table 1 Thermal chemical data related to the formations of $YFeO_3$ and $Y_3Fe_5O_{12}$

Reaction	Gibbs free energy (ΔG^0_{1473}, kJ/mol)
$3Fe(s) + 2O_2(g) = Fe_3O_4(s)$	-653.1[20]
$2Fe(s) + 3/2O_2(g) = Fe_2O_3(s)$	-447.7[20]
$Fe(s) + 1/2Y_2O_3(s) + 3/4O_2(g) = YFeO_3(s)$	-250.2[19]
$5Fe(s) + 3/2Y_2O_3(s) + 15/4O_2(g) = Y_3Fe_5O_{12}(s)$	-1208.8[19]
$3YFeO_3(s) + 2/3Fe_3O_4(s) + 1/6O_2(g) = Y_3Fe_5O_{12}(s)$	-27.2[19]

Mechanism A

$$3/2Y_2O_3(s) + 5/2Fe_2O_3(s) = Y_3Fe_5O_{12}(s)$$
$$\Delta G^0_{1473} = -89.5 \text{ kJ/mol} \quad (1)$$

$$1/5Y_3Fe_5O_{12}(s) + 1/5Y_2O_3(s) = YFeO_3(s) \text{ (rds)}$$
$$\Delta G^0_{1473} = -8.4 \text{ kJ/mol} \quad (2)$$

Mechanism B

$$1/2Y_2O_3(s) + 1/2Fe_2O_3(s) = YFeO_3(s)$$
$$\Delta G^0_{1473} = -26.4 \text{ kJ/mol} \quad (3)$$

$$3YFeO_3(s) + Fe_2O_3(s) = Y_3Fe_5O_{12}(s) \text{ (rds)}$$
$$\Delta G^0_{1473} = -15.1 \text{ kJ/mol} \quad (4)$$

In mechanism B, the conversion of $YFeO_3$ to $Y_3Fe_5O_{12}$ was proved by Kimizuka *et al.* to be very slow[19] and therefore, it was supposed to be the rate-determing step (rds). Mechanism A is more favorable than mechanism B because (1) Gibbs free energy change for the formation of $Y_3Fe_5O_{12}$ (Eq. 1) is more negative than that of $YFeO_3$ (Eq. 3) implying that the formation of $Y_3Fe_5O_{12}$ is easier than that of $YFeO_3$; (2) if mechanism B is reasonable, Y_2O_3 and $Y_3Fe_5O_{12}$ should not coexist if the sample is stoichiometric according to the phase diagram of Y_2O_3-Fe_2O_3-O_2 system.[21] The XRD patterns of $YFeO_3$ with different heating histories as shown in Fig. 1 clearly demonstrate that the intermediate products are Y_2O_3 and $Y_3Fe_5O_{12}$, strongly supporting that the mechanism A is correct. In order to synthesize $YFeO_3$ without notable existence of Y_2O_3 and $Y_3Fe_5O_{12}$, the sintering time at 1350℃ should be longer than 15 h or at higher temperatures if the solid state reaction method is applied.

XRD analysis confirms that those compounds $Y_{1-x}Ca_xFe_{1-y}Mn_yO_{3-\delta}$ with $x \leq 0.1$ and $y \leq 0.4$ are of single phases with orthorhombic structure of $YFeO_3$ (Fig. 1). Ca^{2+} and Mn^{3+} are surely introduced to the Y^{3+} and Fe^{3+} sites respectively due to their similar radii and electronic states.

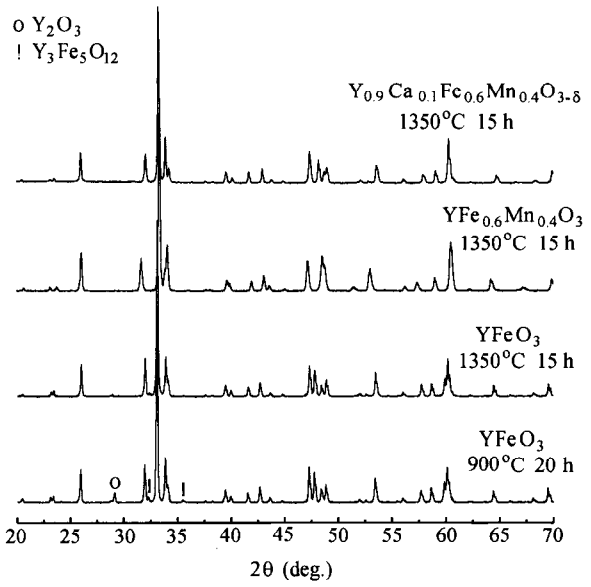

Fig. 1 XRD patterns of $YFeO_3$, $YFe_{0.6}Mn_{0.4}O_3$ and $Y_{0.9}Ca_{0.1}Fe_{0.6}Mn_{0.4}O_{3-\delta}$.

Valence distribution of Fe *in* $YFeO_3$

In this paper, Kröger-Vink notations have the following meanings: $Fe_{Fe}^{\times} = Fe^{3+}$, $Fe'_{Fe} = Fe^{2+}$ and $Fe_{Fe}^{\cdot} = Fe^{4+}$; when Fe^{3+}-sites are replaced by Mn^{3+}, Mn^{2+} or Mn^{4+}, then $Mn_{Fe}^{\times} = Mn^{3+}$, $Mn'_{Fe} = Mn^{2+}$, $Mn_{Fe}^{\cdot} = Mn^{4+}$; $Ca'_{Y} = Ca^{2+}$ if Y^{3+} is replaced by Ca^{2+}.

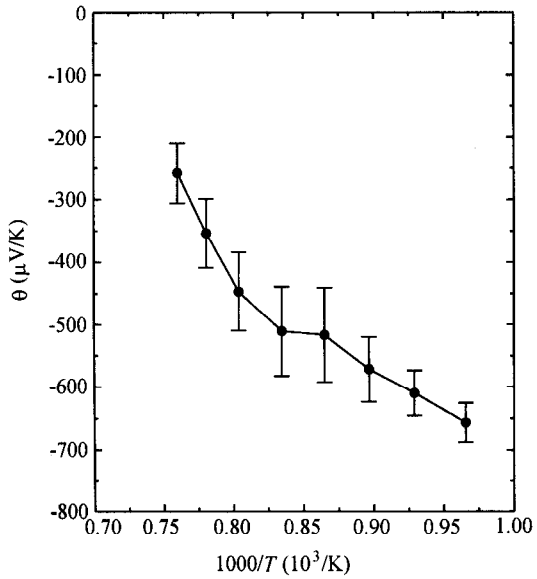

Fig. 2 Seebeck-coefficient (θ) of $YFeO_3$, air atmosphere.

In Fig. 2 is shown the thermal power of $YFeO_3$ measured in air atmosphere. In the whole experimental temperature range, $YFeO_3$ shows the n-type conductivity. The Seebeck-coefficient (θ) can be calculated with the following equation:[1,8]

$$\theta = \pm \frac{k}{e}[\ln(\frac{2(1-c)}{c})] + S_0 \qquad (5)$$

were e is the charge of electron, k is Boltzman constant, S_0 is the vibration entropy per particle and is often neglected due to its small value,[1] the factor of 2 takes into account the spin-degeneracy and c is the charge-carrier concentration. Because $YFeO_3$ shows n-type conductivity, it is assumed that electrons associated with the formation of Fe^{2+} are charge-carriers as proposed in the system Fe_3O_4 which also shows n-type conductivity.[14] Fe^{2+} in $YFeO_3$ is formed by the thermal disproportionation $2Fe^{3+} = Fe^{4+} + Fe^{2+}$. The valence distribution of Fe based on the calculation of Eq. 5 is shown in Fig. 3. c is equal to 0.03 at 1000℃, indicating that only 3% of Fe-sites in $YFeO_3$ contribute to the electrical conductivity.

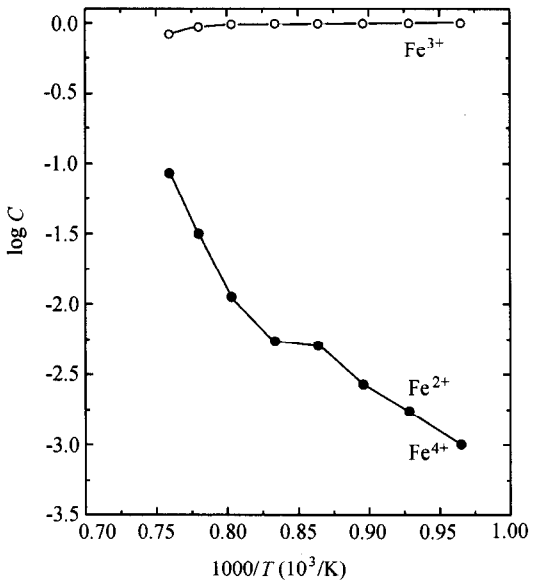

Fig. 3 Valence distribution of Fe in $YFeO_3$, air atmosphere, C = concentration.

The electrical conductivity of $YFeO_3$ as a function of oxygen partial pressure is shown in Fig. 4. In the isotherm diagram, the conductivity can be clearly distinguished into two parts. In the high oxygen partial pres-

sure region, the conductivity is constant and it increases in the low oxygen partial pressure region. The main defect structure of undoped $YFeO_3$ is analyzed by the following equilibrium equations:

$$e' + h^{\cdot} = 0 \qquad K_i = np \tag{6}$$

$$O_O^{\times} = V_O^{\cdot\cdot} + O_i'' \qquad K_F = [V_O^{\cdot\cdot}][O_i''] \tag{7}$$

$$O_O^{\times} = \frac{1}{2}O_2 + V_O^{\cdot\cdot} + 2e \qquad K_{OX} = P_{O_2}^{1/2}[V_O^{\cdot\cdot}]n^2 \tag{8}$$

$$\text{or} \quad \frac{1}{2}O_2 = O_i'' + 2h^{\cdot} \qquad K_{OX} = [O_i'']P^2P_{O_2}^{-1/2} \tag{9}$$

$$2[O_i''] + n = 2[V_O^{\cdot\cdot}] + P \tag{10}$$

$$\delta = [V_O^{\cdot\cdot}] - [O_i''] \tag{11}$$

Notations in the above equations have the following meanings: $n + [e'] = [Fe'_{Fe} - Fe^{\times}_{Fe}]$, h = hole, $p = [h^{\cdot}] = [Fe^{\cdot}_{Fe} - Fe^{\times}_{Fe}]$, [] = concentration, $O_O^{\times}$ = normal oxygen atom in the crystal lattice, $V_O^{\cdot\cdot}$ = oxygen vacancy, O_i'' = interstitial oxygen atom, P_{O_2} = oxygen partial pressure, δ = stoichiometry deviation of oxygen.

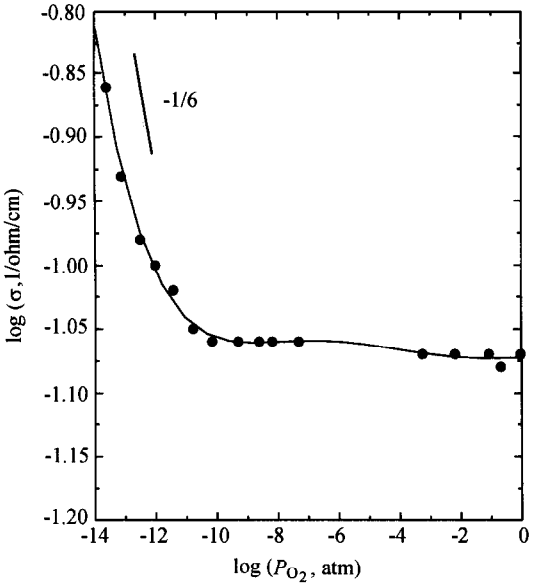

Fig. 4 Electrical conductivity (σ) of $YFeO_3$ as a function of oxygen partial pressure (P_{O_2}).

High oxygen partial pressure region

In this region, the total conductivity is constant. Assuming $n = p$, then we obtain:

$$K_i = np = n^2 = p^2 \tag{12}$$

$$[V_O^{\cdot\cdot}] = K_{OX}n^{-2}P_{O_2}^{-1/2} = K_{OX}K_i^{-1}P_{O_2}^{-1/2} \tag{13}$$

$$[O_i''] = K_F/[V_O^{\cdot\cdot}] = K_FK_iK_{OX}^{-1}P_{O_2}^{1/2} \tag{14}$$

$$\delta = K_F^{1/2}\{(\frac{P_{O_2}}{P_{O_2}^*})^{-1/2} - (\frac{P_{O_2}}{P_{O_2}^*})^{1/2}\} \tag{15}$$

$P_{O_2}^*$ is the critical oxygen partial pressure at which $\delta = 0$.

Low oxygen partial pressure region

In this region, the formation of $V_O^{\cdot\cdot}$ is electrically compensated by the formation of e', *i.e.* $2[V_O^{\cdot\cdot}] = n$. The following equations can be obtained:

$$[V_O^{\cdot\cdot}] = (K_{OX}/4)^{1/3}P_{O_2}^{-1/6} \tag{16}$$

$$[O_i''] = K_F(4/K_{OX})^{1/3}P_{O_2}^{1/6} \tag{17}$$

$$n = (2K_{OX})^{1/3}P_{O_2}^{-1/6} \tag{18}$$

$$p = K_i(2K_{OX})^{-1/3}P_{O_2}^{1/6} \tag{19}$$

$$\delta = K_F^{1/2}\{(P_{O_2}/P_{O_2}^*)^{-1/6} - (P_{O_2}/P_{O_2}^*)^{1/6}\} \tag{20}$$

Equilibrium constants K_i, K_{OX} and K_F can be obtained from the experimental data of thermal gravimetric analysis (TGA) of $YFeO_3$. Based on the experimental data of TGA,[22] $P_{O_2}^*$ could be calculated to be 4.6×10^{-4} atm at 1000℃, then these equilibrium constants at 1000℃ are: $K_i = (9.8 \pm 3.5) \times 10^{-9}$, $K_{OX} = (2.4 \pm 1.3) \times 10^{-13}$, and $K_F = (2.4 \pm 0.9) \times 10^{-9}$. Fig. 5 shows the valence distribution of Fe as a function of oxygen partial pressure at 1000℃, which is obtained with the above equilibrium constants.

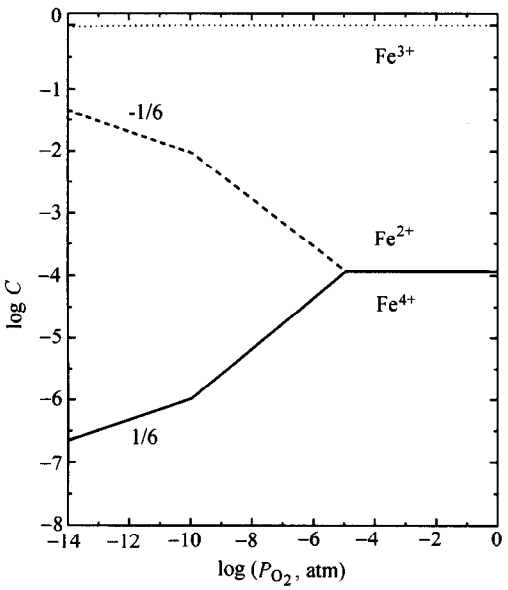

Fig. 5 Valence distribution of Fe in $YFeO_3$ as a function of oxygen partial pressure (P_{O_2}), C = concentration.

Valence distribution of Mn *in* $YFe_{0.6}Mn_{0.4}O_3$ *and* $Y_{0.9}Ca_{0.1}Fe_{0.6}Mn_{0.4}O_{3-\delta}$

The formation of stable ferrates of Fe^{4+} can only occur under high oxygen pressure.[23] In $CaMn_{1-x}Fe_xO_{3-\delta}$, all Fe-sites are in valence Fe^{3+} and most of Mn-sites in Mn^{4+},[24,25] implying that Fe^{4+} is more oxidizing and unstable than Mn^{4+}. In $YFe_{0.6}Mn_{0.4}O_3$ and $Y_{0.9}Ca_{0.1}Fe_{0.6}Mn_{0.4}O_{3-\delta}$, Fe^{3+} is also supposed to be the only oxidation state of Fe-sites. The disproportionation $2Mn^{3+} = Mn^{2+} + Mn^{4+}$ is an automatic process because the electrode potential E^o (Mn^{4+}/Mn^{3+}, 0.95 V) is much lower than E^o(Mn^{3+}/Mn^{2+}, 1.51 V), and then Mn-sites may have three oxidation states, *i.e.* Mn^{2+}, Mn^{3+} and Mn^{4+}.

In air atmosphere, both $YFe_{0.6}Mn_{0.4}O_3$ and $Y_{0.9}Ca_{0.1}Fe_{0.6}Mn_{0.4}O_{3-\delta}$ show the p-type conductivity below 950℃ and 920℃ respectively (Fig. 6). The conductivity mechanism $Mn^{3+} \Leftrightarrow Mn^{4+}$ is more reasonable than other mechanisms such as $Fe^{3+} \Leftrightarrow Mn^{4+}$, $Fe^{3+} \Leftrightarrow Mn^{3+}$, $Fe^{3+} \Leftrightarrow Mn^{2+}$ and $Mn^{3+} \Leftrightarrow Mn^{2+}$ which have already been proved in many other works.[13] The conductivity type of mechanism $Mn^{3+} \Leftrightarrow Mn^{4+}$ is dependent on the concentration ratio of Mn^{3+} and Mn^{4+}.[5] The function of $YFeO_3$ is only to support the orthorhombic perovskite-structure, both Fe^{3+} and Mn^{2+} sites act as site-blockers. In $YFe_{0.6}Mn_{0.4}O_3$, [Mn^{4+}] is equal to [Mn^{2+}] and oxygen vacancy in air atmosphere is not taken into account. In $Y_{0.9}Ca_{0.1}Fe_{0.6}Mn_{0.4}O_{3-\delta}$, to maintain the electrical neutrality condition is needed. The valence distribution of Mn calculated with Eq. (5) is shown in Fig. 7.

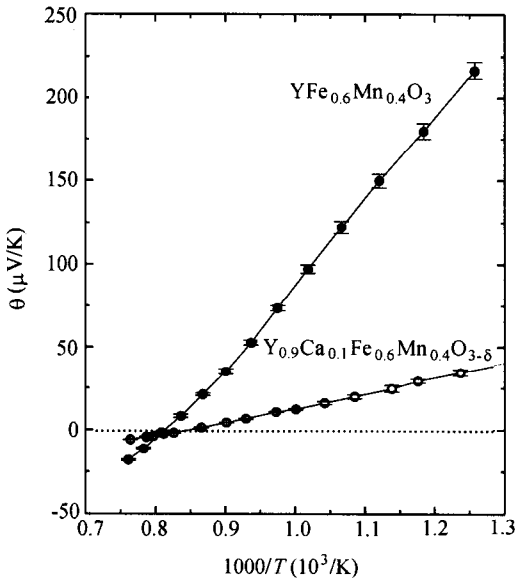

Fig. 6 Seebeck-coefficient (θ) of $YFe_{0.6}Mn_{0.4}O_3$ and $Y_{0.9}Ca_{0.1}Fe_{0.6}Mn_{0.4}O_{3-\delta}$, air atmosphere.

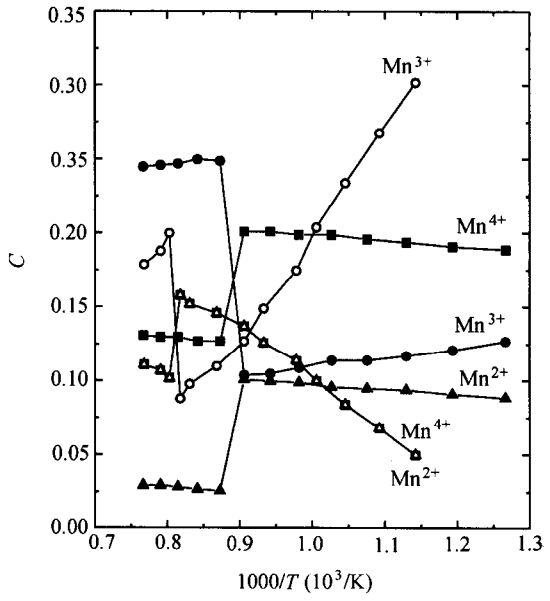

Fig. 7 Valence distribution of Mn in $YFe_{0.6}Mn_{0.4}O_3$ (open symbols) and $Y_{0.9}Ca_{0.1}Fe_{0.6}Mn_{0.4}O_{3-\delta}$ (solid symbols), air atmosphere, C = concentration.

Both $YFe_{0.6}Mn_{0.4}O_3$ and $Y_{0.9}Ca_{0.1}Fe_{0.6}Mn_{0.4}O_{3-\delta}$ decompose under oxygen partial pressure lower than 1×10^{-8} atm at 1000℃, and they do not exhibit the required oxygen-activity-dependence behavior, no information about the valence distribution under low oxygen partial pressure could be obtained.

So far, the reason for the transition of conductivity type of $YFe_{0.6}Mn_{0.4}O_3$ and $Y_{0.9}Ca_{0.1}Fe_{0.6}Mn_{0.4}O_{3-\delta}$ is not clear. One possibility is the change of crystal structure at high temperatures. When the structure of Mn_3O_4 changes at high temperature, both the conductivity and valence distribution change dramatically.[13]

Acknowledgment

Part of work of this paper was finished in the Department of Inorganic Materials & Engineering, Seoul National University of Korea with the help of Prof. H.-I. Yoo and Dr. C.-S. Kim. Great thanks to Mr. P. Lersch of Forschungszentrum Juelich of Germany for XRD measurement.

References

1 Yoo, H.-I.; Kim, C.-S. *Solid State Ionics* **1992**, *53*, 583.
2 Park, H.-B.; Kweon, H.-J.; Hong, Y.-S.; Kim, S.-J.; Kim, K. *J. Mater. Sci.* **1997**, *32*, 57.
3 Fu, B.; Huebner, W.; Trubelja, M. F.; Stubican, V. S. *The 3rd Inter. symp, Solid Oxide Fuel Cell*, Honolulu, May **1993**, p. 276
4 Kim, C.-S.; Yoo, H.-I. *J. Electrochem. Soc.* **1996**, *143*, 2863.
5 Stevensen, J. W.; Nasrallah, M. M.; Anderson, H. U.; Sparlin, D. M. *J. Solid State Chem.* **1993**, *102*, 157.
6 Weber, W. J.; Griffin, C. W.; Bates, J. L. *J. Am. Ceram. Soc.* **1987**, *70*, 265.
7 Raffaelle, R.; Anderson, H. U.; Sparlin, D. M.; Parris, P. E. *Phys. Rev. Lett.* **1990**, *65*, 1383.
8 Raffaelle, R.; Anderson, H. U.; Sparlin, D. M.; Parris, P. E. *Phys. Rev. B* **1991**, *43*, 7991.
9 Tai, L.-W.; Nasrallah, M. M.; Anderson, H. U.; Sparlin, D. M.; Sehlin, S. R. *Solid State Ionics* **1995**, *76*, 259; 273.
10 Stevenson, J. W.; Armstrong, T. R.; Carneim, R. D.; Pederson, L. R.; Weber, W. J. *J. Electrochem. Soc.* **1996**, *143*, 2722.
11 Lankhorst, M. H. R.; Elshof, J. E. *J. Solid State Chem.* **1997**, *130*, 302.
12 Cao, X. Q.; Kim, C. S.; Yoo, H. I. *J. Am. Ceram. Soc.* **2001** (in press).
13 Dorris, S. E.; Mason, T. O. *J. Am. Ceram. Soc.* **1988**, *71*, 379.
14 Mason, T. O.; Bowen, H. K. *J. Am. Ceram. Soc.* **1981**, *64*, 237.
15 Erickson, S.; Mason, T. O. *J. Solid State Chem.* **1985**, *59*, 42.
16 Trestman-Matts, A.; Dorris, S. E.; Kumarakrishnan, S.; Mason, T. O. *J. Am. Ceram. Soc.* **1983**, *66*, 829.
17 Carter, D. C.; Mason, T. O. *J. Am. Ceram. Soc.* **1988**, *71*, 213.
18 Navrotsky, A.; Kleppa, O. J. *J. Inorg. Nucl. Chem.* **1967**, *29*, 2701.
19 Kimizuka, N.; Yamamoto, A.; Ohashi, H. *J. Solid State Chem.* **1983**, *49*, 65.
20 Samsonov, G. V. *The Oxide Handbook*, IFI/Plenum-New York, Washington-London, **1982**.
21 Cassedanne, J., in *Phase Diagrams for Ceramists Volume IV*, Eds: Roth, R. S.; Negas, T.; Cook, L. P., The American Ceramic Society Inc., **1981**, Fig. 4212 on p.44.
22 Kim, C.-S. *Ph. D Thesis*, Seoul National University of Korea, Seoul, **1998**.
23 Poulsen, F. W.; Lauvstad, G.; Tunold, R. *The 9th Solid State Ionics Conference*, Hague, Sept. Hague, **1993**. p.1.
24 Fontcuberta, J.; Crusellas, M. A.; Rodríguez-Carvajal, J.; Vallet, M.; Alonso, J.; González-Calbet, J. *J. Solid State Chem.* **1989**, *83*, 150.
25 Battle, P. D.; Davison, C. M.; Gibb, T. C.; Vente, J. F. *J. Mater. Chem.* **1996**, *6*, 1187.

(E200004098 SONG, J.P.; DONG, L.J.)